Parallel Atomic Force Microscopy and NMR Spectroscopy To Investigate Self-Assembled Protein−Nucleotide Aggregates

Jan K. Rainey and M. Cynthia Goh*

Department of Chemistry, University of Toronto, Toronto, Ontario, Canada M5S 3H6

Received: November 28, 2001; In Final Form: March 20, 2002

The concurrent use of atomic force microscopy (AFM) and NMR spectroscopy should enable one to link the structural information from the former to chemical information obtained with the latter. In this instance, the self-assembly of type I collagen into segmental long spacing (SLS) collagen crystallites is examined, and the first concrete evidence for the incorporation of the nucleotide ATP into these crystallites is presented. The type I collagen monomer contains no phosphorus, unlike the triphosphate group of the ATP, thus making ^{31}P NMR spectroscopy a highly specific probe for the location and interaction of ATP. The changes in the ^{31}P NMR spectral attributes upon self-assembly of SLS collagen crystallites under various conditions are interpreted with relation to the crystallite morphology observed with AFM. The formation of crystallites is found to correlate with decreased mobility of all three ^{31}P nuclei of ATP, as evinced by appreciable line broadening in the solution-state spectra. This is attributable to ATP incorporation into the crystallite structure. Analysis of the resonance frequencies for each of the ^{31}P nuclei of ATP indicates that the α- and γ-phosphates have decreased electron density relative to the β-phosphate upon incorporation, implying direct charge−charge binding, with binding probabilities greater for the α- and γ-phosphate groups than for the β-phosphate group. Three possible scaffolding roles of the ATP are proposed with respect to the structure of the SLS collagen crystallite based upon the evidence presented.

1. Introduction

The direct combination of nuclear magnetic resonance (NMR) spectroscopy and atomic force microscopy (AFM) can potentially be quite useful for a wide variety of systems, since it would allow for the linkage of mesoscale structural information from AFM to chemical information obtained by NMR. Of particular interest and applicability are systems of a macromolecular, supramolecular, or colloidal nature, as these may be readily examined by both techniques. For these systems, NMR spectroscopy becomes challenging because of the sheer number of potential resonance signals. Highly elegant techniques have been developed in order to overcome the problems associated with such samples; however, their employment is far from routine.[1−4] Conversely, examination of these samples, which are 1 nm or more in size, by AFM is relatively straightforward.[5−9] In this paper, AFM analysis of a supramolecular complex made of protein and nucleotide components is used to facilitate the interpretation of NMR spectroscopic information, shedding new light upon a long studied system: the segmental long spacing (SLS) collagen crystallite.

In NMR spectroscopy, the measured signals are produced by the ensemble of all sensitive nuclei within a sample. Information regarding specific chemical environments within complex systems, such as the SLS protein aggregate, may thus be obtained;[4] however, NMR derived structural information in such large biomolecular systems is more challenging to produce.[1,2,4] With AFM, the surface morphology of specific aggregates may be readily observed, potentially to sub-Angstrom resolution.[5−9] While stunning images may thus be produced,

identification of the exact chemical nature of the species being imaged is extremely difficult, if at all possible. The information thus obtained, while it may be up to Angstrom-scale resolution, reflects simply the surface topography. Nevertheless, species from many portions of a sample can be readily imaged, and quantitative measurements of their surface features carried out. The direct combination of the species explicit chemical information from NMR spectroscopy with the intimate structural and morphological detail from AFM will provide complementary information, given the appropriate experimental design.

Preferential aggregation of proteins into complex but well-defined structures is a ubiquitous phenomenon in a variety of natural and pathological processes. In some cases, species other than the protein undergoing aggregation may be involved in the process, while, in others, only the protein itself is involved. Extensive biophysical and chemical analysis employing disparate methodologies has been carried out on both assembly pathways and their end products. Typical systems that have been subjected to this type of analysis are amyloid fibrils,[10] the extracellular matrix,[11−13] muscle tissue,[14] and paired helical filaments.[15] The fibril-forming collagens may self-assemble into various constructs of differing morphologies and dimensions.[13,16−20] The preferential formation of such structures may be induced in vitro via different assembly conditions. While factors such as temperature[21] and addition of noncollagenous species[16,22−25] contribute heavily to the nature of the collagenous structure formed, the surface charge and chemical properties of the collagen monomer itself seem to be essential factors.[26,27]

Collagen is typically associated with fibrillar structures microns in length. However, a curious construct, termed the segmental long-spacing (SLS) collagen crystallite, self-assembles upon the incubation of acidified collagen monomer with

* To whom correspondence should be addressed. Phone number: (416) 978-6254. Fax number: (416) 978-4526. E-mail: cgoh@alchemy.chem.utoronto.ca.
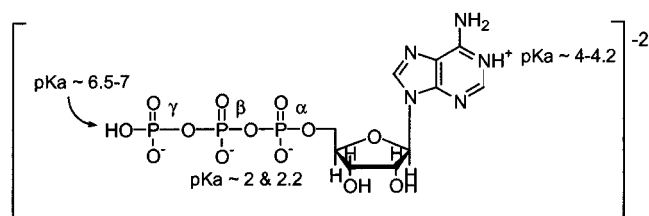
Figure 1. Structure of adenosine 5′-triphosphate (ATP) at pH < 4 with α, β, and γ phosphorus nuclei labeled and pK_a's given[31-33] for ionizable groups.

a nucleotide such as adenosine 5′-triphosphate (ATP).[24,25] The assembly process is somehow limited to two dimensions, forming cylindrical structures of length corresponding exactly to that of the collagen monomer, i.e., ~280 nm for type I collagen, and diameters on the order of 50−100 nm. Previous studies[25] have concentrated heavily upon the morphology and surface characteristics of these constructs. There has been an underlying assumption that ATP is incorporated directly into the crystallite since its discovery by Schmitt et al.,[24] but no direct evidence supports this assumption, or the nature of the incorporation. A transmission electron microscopy study by Kobayashi and co-workers is suggestive of ATP incorporation within the crystallite;[28] however, the evidence presented is by no means conclusive. Despite sporadic bursts of study over the last 50 years, the role of ATP, both in the assembly process and in the stabilization of the crystallite structure, remains enigmatic.

Investigation into the abilities of polyanions other than ATP to form SLS collagen have shown the necessity of the triphosphate moeity.[20,29] Not only is the diphosphate moiety of adenosine-5′-diphosphate unable to induce SLS collagen formation,[20,29] but a variety of alternate structures are observed[30] as the pH in collagen−ATP mixtures is increased. Furthermore, there is no evidence that ATP hydrolysis is taking place.[20,25,29] These findings imply the importance of the tri-anionic charge state[31-33] in the triphosphate group expected at acidic pH (Figure 1).

Light scattering studies have shown that SLS crystallites require a critical concentration of ATP, below which no increase in scattering is observed upon incubation of collagen monomer with ATP.[29,34] The molar ratio of ATP to collagen at this point is about 900 to 1. Note that there is uncertainty in this value because of the difficulty in determining the actual concentration of collagen monomers (vs oligomers, fibrils, or nonspecific aggregates) in solution.[35-39] Structural studies by AFM indicated that this critical ratio of ATP to collagen (hereafter denoted $r*$) is linked with the boundary between formation of "partial" vs "complete" SLS crystallites: Below $r*$, crystallites of varying, smaller diameters are seen.[29,34] Above $r*$, the typical SLS crystallites with fairly uniform diameter (~100−150 nm in solution, calculated from light scattering experiments[29]) and morphology[20,29] are observed. Thin, filamentous collagenous structures are typically observed alongside SLS collagen both below and above $r*$. Why there is such a uniformity in size of SLS crystallites remains a puzzle, but since this is only achieved once the critical ATP to collagen ratio is surpassed, we propose there to be excess ATP in solution once $r*$ is surpassed.[29,34]

Typical NMR studies of collagen systems have concentrated on model peptides, as opposed to full monomers or assembled collagenous constructs.[40] This is due primarily to the large size of the collagen monomer (type I collagen contains ~3150 amino acid residues[41,42]) and its highly uniform triple-helical[43-45] secondary structure composed of 33% glycine and ~22% proline

or hydroxyproline.[42] These features make ^{1}H, ^{13}C, or ^{15}N NMR spectroscopy of the collagen monomer extremely challenging, due to the massive amount of peak overlap. However, the type I collagen monomer contains no phosphorus. This fact is exploited in our work, in that only the nucleotide components in the SLS collagen system will give rise to the ^{31}P NMR signal, providing a highly specific probe for the nucleotide component. When combined with structural information obtained by AFM concerning the expected limited or excess state of ATP, the two techniques prove highly complementary.

2. Materials and Methods

2.1. Assembly of Segmental Long-Spacing Collagen Crystallites. Type I calf-skin collagen and ATP were obtained from Sigma (St. Louis, MO) and deuterated solvents from Cambridge Isotopes (Cambridge, MA). Type I calf-skin collagen was dissolved (~2 mg/mL) in deuterated ~8.3 mM acetic acid (0.05% v/v) solution, shaken, and allowed to dissolve for several hours at 4 °C. All collagen concentrations reported after this point are relative to this initial dissolved amount. To remove insoluble aggregates from the suspension, it was centrifuged for 1 h at 15000g and 4 °C, producing a clear, relatively viscous solution and a cloudy pellet. Immediately prior to use, the supernatant was filtered through a 0.45 μm filter (Millex-HV durapore membrane filter, Millipore, Bedford, MA) in order to remove large aggregates from solution. Collagen monomer was mixed with ATP (disodium salt, bacterial source at >99% purity) to final concentrations of ~1 and ~1.8 mg/mL, respectively, in deuterated 0.05% acetic acid (v/v in D$_2$O) at pH ~3.8. The molar ratio of ATP (MW 551.1 g/mol) to collagen (MW ~280 kDa) is ~925:1 at the 1.8 to 1 mg/mL ratio. Note that the actual ratio is likely higher due to the expected loss of collagen that has aggregated and been removed during the centrifugation and filtration processes. This solution was incubated at room temperature for ~6 h. Assembled SLS collagen crystallites produce a cloudy, viscous solution.

2.2. Denaturation of Collagen Sample. A heat-denatured collagen sample was produced by carrying out the initial centrifugation step at ~55 °C. The resulting supernatant was cooled to 4 °C, filtered, and subjected to the identical conditions used for SLS crystallite assembly at concentrations of 1.8 mg/ mL ATP and ~1.0 mg/mL denatured collagen.

2.3. ^{31}P NMR Spectroscopy. Solution-state NMR spectroscopy was carried out on 300 MHz (^{1}H frequency) Varian Mercury and Gemini spectrometers, operating at frequencies of 121.47 or 121.46 MHz, respectively, for [31]P. Deuterium shimming was performed by the gradient method in the former case, and manually in the latter case. Samples were examined in 5 mm NMR tubes, and broad-band [1]H-decoupled spectra were acquired at room temperature (25.0 °C). Acquisition parameters were adapted from those employed by Marsolais et al.[46] A repetition time of 2.0 s and an acquisition time of 1.3 s were employed with a 45° pulse. An external standard of 85% H$_3$-PO$_4$ was employed. The sample was first shimmed and locked on the deuterium signal. The external standard was then inserted, and the spectral offset was modified as appropriate (typically, on the order of 0.1−0.3 Hz). The sample was reinserted, and no further changes were made to the lock, shim, or offset. The number of transients used was dependent upon the spectrometer time available. Line broadening of 1 Hz and zero-filling on the order of 2−3 times the collected data points were employed during Fourier transformation.

2.4. Analysis of ^{31}P NMR Signal Line Broadening. The raw, free induction decay file in the Varian VNMR format was

AFM and NMR of Protein−Nucleotide Aggregates

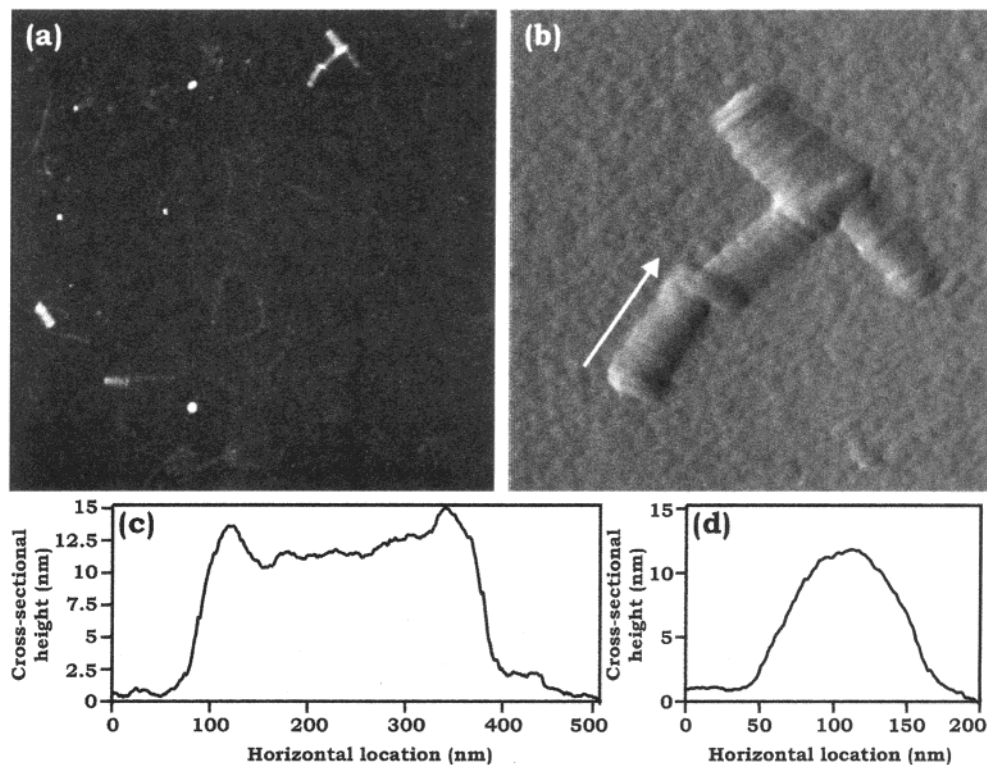*J. Phys. Chem. B, Vol. 106, No. 21, 2002* **5555**

Figure 2. AFM images of typical areas of SLS collagen samples assembled below the critical ATP-to-collagen ratio: (a) contact mode height image, 6 μm × 6 μm (height scale: black, 0 nm; white, 50 nm); (b) deflection image, 1 μm × 1 μm). The longitudinal section (c) was taken parallel to the arrow in (b) along the middle of the crystallite, while the cross-section (d) was taken perpendicular to the arrow at the center of the crystallite.

imported into MestRe-C 2.1.0 (MS-Windows freeware available from the Universidad de Santiago de Compostela, Spain, at http://qobrue.usc.es/jsgroup/MestRe-C/MestRe-C.html). Fourier transformation was carried out with the same parameters as on the Varian VNMR software, to produce spectra with identical attributes. The spectral data were exported in ASCII format to Origin 5.0 (Microcal Software Inc., Northampton, MA). Each of the three ^{31}P phosphate peaks was plotted separately for a given sample and fitted to a single (β-phosphate), double- (α- and γ-phosphates), or quadruple-Lorentzian (β-phosphate) shape. The line width at half-maximum for each set of ^{31}P peak of a phosphate group of the ATP was determined by averaging all line widths for a given multiple-Lorentzian fit. Comparison to the center-of-mass weighted peak resonance frequency from VNMR and to a calculated center-of-mass was also carried out to ensure that the Lorentzian fits were reasonable and all resonance frequency shift calculations employed these center-of-mass resonance values.

2.5. Preparation of Atomic Force Microscopy Samples. Sample stubs were prepared by attaching a sheet of mica (∼75 mm × 75 mm) with an electron microscopy locator grid affixed between the stub and the mica to allow for repeat imaging of the same sample region.[47] The mica was freshly cleaved just prior to application of the sample. Samples (10 μL aliquot) were applied, neat or immediately upon dilution in 0.45 μm filtered deionized water, directly to the mica surface and dried under cover at ambient temperature and pressure.

2.6. Atomic Force Microscopy. Contact mode or Tapping-Mode imaging was carried out using either a Nanoscope III (Digital Instruments, Santa Barbara, CA) or Solver P47 (NT-MDT, Moscow, Russia) scanning probe microscope. For contact mode imaging, silicon nitride square pyramidal cantilevers of spring constant 0.58 N/m (Nanoprobe, Digital Instruments) were employed. Both height and deflection mode images were collected simultaneously for contact mode with both instruments.

In the case of TappingMode imaging, ultrasharp conical silicon tips of reported length 90 μm and a radius of curvature of less than 10 nm at the tip (SC-12 series, NT-MDT) were employed. These tips had a typical resonance frequency of ∼320 kHz and nominal spring constant of ∼14 N/m. Height mode images were collected along with either an amplitude or phase image. A scan rate of 2−4 Hz was typically sufficient to afford good signal-to-noise ratio, with the lower rates required as the resolution is increased. To minimize tip artifacts, imaging was repeated using different tips. Only features that were reproducible from tip-to-tip are reported. Images were typically software plane-fit in order to alleviate piezoelectric scanner nonlinearity from the image by plane-fits of featureless regions of the height image. No other postacquisition processing was carried out. These plane-fit images were employed for quantitative analysis, such as cross-sectional analysis. All images shown are representative of the sample as a whole; multiple aliquots were imaged in each case, with a variety of areas examined for consistent sample morphology.

3. Results

3.1. AFM Imaging of SLS Collagen Crystallites. Transmission electron microscopy of SLS collagen crystallites indicate cylindrical symmetry,[25] while AFM images of sample deposited on mica show a flattened structure, which is ascribed to interaction between the sample and the substrate.[17,20,29] Some variation is seen in protein adsorption with differing substrates;[48] however, due to the well-characterized nature of the SLS crystallite on mica,[17,20,29] we have chosen to employ mica exclusively as our flat substrate for AFM imaging in this particular study. Representative dry AFM images of crystallites assembled in deuterated acetic acid solution are shown in Figures 2 and 3, along with longitudinal sections (along the main axis) and cross-sections (perpendicular to the main axis). While the
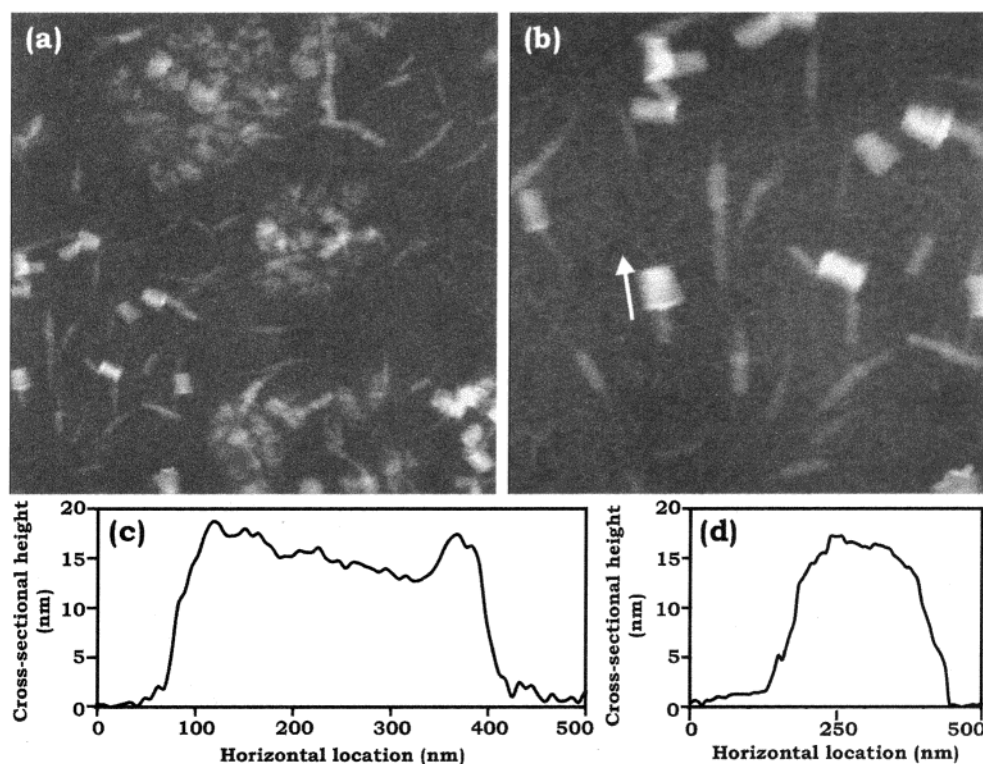
Figure 3. Typical areas of an SLS collagen sample assembled with excess ATP relative to collagen monomer imaged by AFM. Contact mode height images: (a) 7 μm × 7 μm (height: black, 0 nm; white, 75 nm); (b) 3.5 μm × 3.5 μm (height: black, 0 nm; white, 45 nm). The longitudinal section (c) was taken parallel to the arrow in (b) along the middle of the crystallite, while the cross-section (d) was taken perpendicular to the arrow at the crystallite center.

interaction with mica tends to flatten the crystallites, it is believed that the general morphology that exists in solution is retained upon deposition and dehydration: The measurements taken along both longitudinal sections and cross-sections correspond well with observations by TEM. Taking into account tip convolution effects[49,50] that increase the measured lateral dimensions by ∼60 nm, the measurements of the long axis of the crystallites are in agreement with the length of a collagen monomer. Furthermore, a reproducible pattern of ridges is observed along this section.

Typical AFM images of SLS collagen crystallites produced below vs above the critical ATP-to-collagen ratio ($r*$ is approximately 900:1, as discussed above) are shown in Figures 2a,b and 3a,b, respectively. In both cases, the longitudinal sections correspond to the monomer length, but the two other dimensions differ. Crystallites formed below $r*$ (Figure 2d) are noticeably smaller, with dimensions of about 10 nm by 70 nm, while those formed above $r*$ (Figure 3d) are much larger, typically 15−70 nm by 200−400 nm. The images shown in Figures 2 and 3 contrast significantly with that of the heat-denatured collagen (Figure 4) incubated with ATP at approximately $r*$. No ordered crystallite superstructures are apparent within the filamentous forms seen. This image is much more typical of that which is observed with gelatinous samples (e.g., ref 51).

Analysis of multiple AFM images such as these obtained either after NMR spectral analysis or at the same time, allowed identification of the type of SLS collagen sample and the proximity to $r*$ in a given set of experiments. Without AFM imaging, we cannot determine the state of SLS crystallites with respect to $r*$. Light-scattering alone is not sufficient, since in cases below $r*$ it is possible that no crystallites at all form. Therefore, microscopic imaging is required to demonstrate the
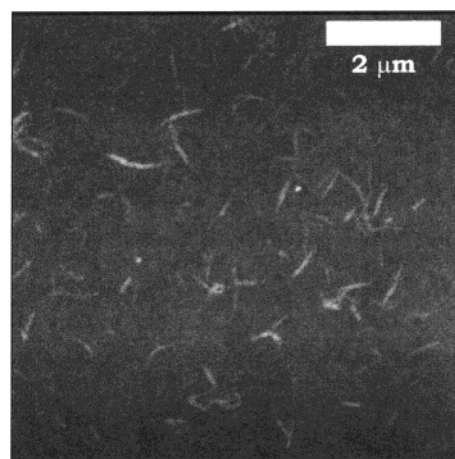

Figure 4. Typical AFM image of sample of denatured collagen incubated with ATP at room temperature for ∼6 h. TappingMode height image. Height: black, 0 nm; white, 25 nm.

formation of these diameter-limited crystallites and readily allows confirmation of the formation of crystallites above $r*$.

3.2. ^{31}P NMR Spectral Attributes. The ^{31}P NMR spectra of typical SLS crystallites produced below $r*$ (AFM image: Figure 2) and above $r*$ (AFM image: Figure 3) are shown in Figure 5a,b, respectively. A characteristic free ATP spectrum is given for comparison in Figure 5d. The ^{31}P NMR spectrum of a heat-denatured collagen sample incubated at approximately $r*$ (AFM image: Figure 3) is given in Figure 4c. The observed splitting and relative locations of the α-, β-, and γ-phosphate peaks (as labeled in Figure 1) correspond well to those reported in the literature (e.g., ref 52). No other ^{31}P NMR signals were observed over the spectral window (−100 to +200 ppm). The γ-phosphate ^{31}P nucleus is always observed at the highest

AFM and NMR of Protein−Nucleotide Aggregates

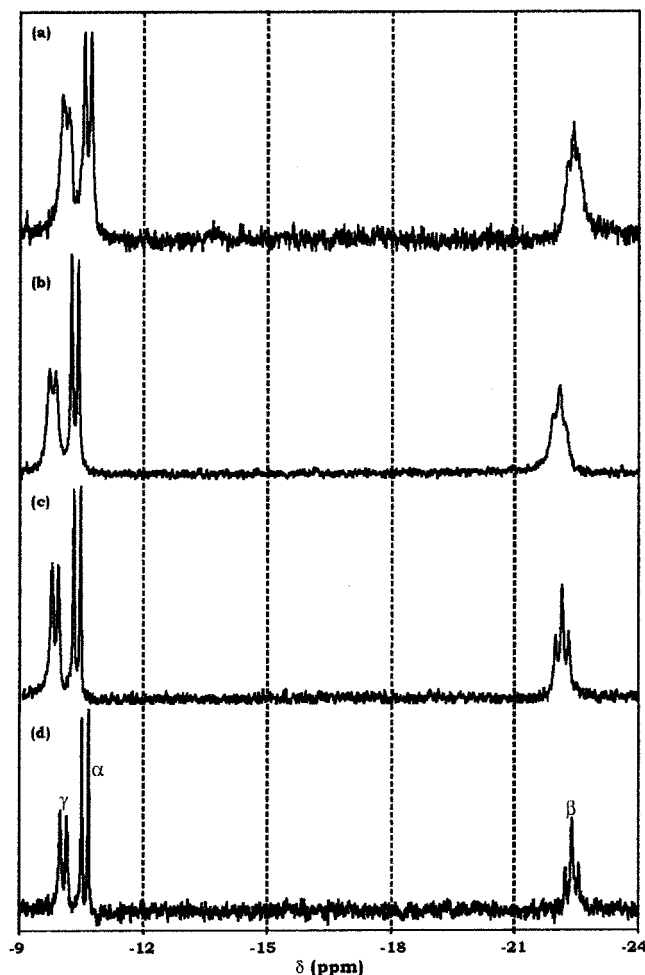*J. Phys. Chem. B, Vol. 106, No. 21, 2002* **5557**

Figure 5. ^{31}P NMR spectra of (a) SLS collagen crystallites formed with limited ATP (23 500 transients). (b) SLS collagen crystallites formed with excess ATP (23 000 transients). (c) ∼1.8 mg/mL ATP incubated with ∼1 mg/mL heat-denatured collagen (11 500 transients). (d) 4.6 mg/mL ATP (3000 transients) All samples in 0.05% deuterated acetic acid (v/v) in D_2O at pH ∼3.8. External standard: 85% H_3PO_4.

TABLE 1: Line Broadening of the ^{31}P NMR Peaks of ATP in Various Segmental Long Spacing (SLS) Collagen Samples

collagen sample (representative spectrum)	relative line broadening[a] of phosphate		
	γ	β[b]	α
SLS collagen, below $r*$ [c] (Figure 5a)	3.0	3.1	2.9
SLS collagen, above $r*$ [d] (Figure 5b)	2.2	2.4	1.9
denatured collagen[e] (Figure 5c)	1.3	2.2	1.4

[a] Average width at half-height for Lorentzian fit of one (β-phosphate) or two (α- and γ-phosphate) peaks, relative to the free ATP (average of two spectra). [b] The β-phosphate line-broadening values are not highly reliable. The given line-broadening factor is from a single Lorentzian fit, which is a bad approximation of the theoretical triplet line shape. Triple- and quadruple-Lorentzians are even less appropriate. [c] Below $r*$, limited ATP. (The value of $r*$ is ∼900 ATP molecules per collagen monomer.) Average of spectra from two different samples. [d] Above $r*$, excess ATP. [e] Heat denatured collagen incubated at $r*$.

TABLE 2: ^{31}P NMR Frequency Differences between the β-Phosphate and the α- and γ-Phosphate Peaks for Free ATP and for Segmental Long Spacing (SLS) Collagen Samples

sample (representative spectrum)	[31]P frequency difference (Hz)[a]		[31]P frequency shift relative to ATP (Hz)[b]	
	α−P to β-P	γ-P to β-P	α-P	γ-P
free ATP[c] (Figure 5d)	1430.0	1493.4	-	-
SLS, below $r*$ [c,d] (Figure 5a)	1434.6	1499.9	+4.6	+6.5
SLS, above $r*$ [d] (Figure 5b)	1432.5	1505.0	+2.5	+11.6
denatured collagen[e] (Figure 5c)	1433.5	1497.3	+3.5	+3.9

[a] Difference between centers-of-mass, calculated using Microsoft Excel, of given ^{31}P peak and the β-^{31}P peak. Signal-to-noise thresholds for were same for all samples. [b] Frequency difference of given ^{31}P peak as compared to the free ATP sample. [c] Average of two spectra from independent samples. [d] Below $r*$, limited ATP. Above $r*$, excess ATP. (Exact $r*$ is ∼900 ATP molecules per collagen monomer.) [e] Heat denatured collagen incubated at $r*$.

resonance frequency (∼10.1 ppm), followed by that of the nearby α-phosphate (∼10.6 ppm), with the β-phosphate being observed at a significantly lower resonance frequency (∼−22.4 ppm). These approximate resonance frequencies are conserved for all of the collagen/ATP spectra shown in Figure 5, as compared to the free ATP spectrum shown. Line broadening of the ^{31}P NMR peaks for the three phosphates of the ATP for both types of SLS collagen and the denatured collagen with ATP are given relative to the free ATP peaks in Table 1, as determined by the line width at half-maximum of the Lorentzian fits for each ^{31}P peak. Finally, the resonance frequencies of the α- and γ-phosphates relative to the β-phosphate for each of the four sample types are summarized in Table 2. Resonance frequency shifts for the entire spectrum (∼20 Hz maximum) from experiment to experiment make any comparison of exact, rather than relative, frequency measures meaningless.

4. Discussion

All NMR spectra of SLS collagen samples were acquired in the solution phase, where the sample of SLS collagen was in deuterated acetic acid. Therefore, all ^{31}P NMR signals arise from the overlapped resonances of any free ATP in solution and any ATP bound, as we will now demonstrate, within SLS collagen crystallites. AFM imaging was carried out upon the identical

samples, deposited upon freshly cleaved mica, and imaged after being allowed to dry at ambient temperature and pressure. The observed SLS collagen structures, while not entirely identical to the conformations in solution, allow the prediction of the degree of free vs bound ATP in solution giving rise to the observed crystallite morphology. Without the AFM evidence, we would be unable to analyze ^{31}P NMR spectral attributes since all peaks are composed of an otherwise unknown combination of free and bound ATP. Keeping these caveats in mind, we will now show the binding of ATP within SLS collagen and its state upon binding.

4.1. ATP Binding within SLS Collagen Crystallites. The formation of SLS crystallites after the addition of ATP to a solution of collagen is heralded by a noticeable change in light scattering or turbidity. Below the critical ATP-to-collagen ratio ($r*$), AFM imaging shows that aggregates are formed that are similar to SLS crystallites, but much smaller in dimension. If the ATP is being incorporated into such structures, it is reasonable to assume that below $r*$, a higher proportion of ATP is bound within the structures than is left free in solution, while above $r*$, the amount of free ATP in solution increases. The spectra in Figure 5 and the observed increase in line broadening (over the free ATP spectrum) summarized in Table 1 can be examined with this view in mind. As the amount of free ATP in solution decreases, the spectral lines for the ^{31}P nuclei of all three phosphates broaden. While it is conceivable that this broadening could simply be due to an increase in solution

viscosity, we will argue that this is in fact due to an increase in the relative amount of bound ATP within the SLS collagen crystallites versus free ATP in solution.

Line broadening in NMR signals is, to a reasonable approximation, inversely proportional to the transverse relaxation time (T_2) plus a term arising from inhomogeneity in the magnetic field experienced by the nucleus in question.[53] (Note that T_2 cannot be readily measured directly through a spin−echo experiment due to the lengthy ^{31}P NMR acquisition times required under the low ATP concentrations needed to prevent gelation of the SLS collagen samples.) The incorporation of ATP within an SLS collagen crystallite will result in a general reduction of its mobility. The mobility of a nucleus has an inverse relationship to its T_2; i.e., a slower nucleus has increased likelihood to exchange spin energy with a neighboring nucleus, therefore decreasing the time required to relax to the ground spin-state. In solid-state NMR,[3,53,54] especially when a quadrupolar nucleus is under investigation (e.g., refs 3 and 54), the magnetic field inhomogeneity throughout a sample may contribute rather distinctly to the line-shape. In our case, however, the SLS collagen crystallites are free to tumble in solution, albeit at a slower rate than free ATP tumbling in solution. Also, ^{31}P has no quadrupolar moment, hence inhomogeneity due to quadrupole orientation differences need not be considered. Because of this, the average magnetic field experienced by the ensemble of all ATP, whether bound within an SLS crystallite or free in solution, should be quite homogeneous. Therefore, in the case of SLS crystallites, line broadening should be due primarily to decreased transverse relaxation times. Our experimental results show increases in line broadening by factors of ∼3 and 2 relative to free ATP for the SLS samples below and above r^*, respectively. This is in agreement with the picture presented: Below r^*, practically all ATP are tied up in the SLS crystallite, and maximal line broadening is expected due to the most efficient transverse relaxation upon restriction of motion. Above r^*, some ATP molecules are bound in the crystallites and undergo transverse relaxation very effectively, while others are free in solution with a correspondingly longer T_2. The average throughout the total ATP population will therefore have a line-broadening intermediate between that of the free ATP and the fully bound (below r^*) ATP.

This interpretation is further supported by the data on the denatured collagen sample incubated with a comparable ratio of ATP molecules per monomer. While some re-formation of the triple-helical secondary structure would likely occur when the sample is cooled following the heat denaturation process, AFM analysis showed no SLS crystallites in this preparation. Therefore, the collagen monomers likely exist as random coils and nonspecific aggregates, which would be much more flexible compared with an SLS crystallite structure. Spectral line broadening was also observed for this sample (Figure 4c; relative to free ATP (Figure 4d) in acetic acid solution) to a factor of ∼1.3−1.4 for both the α- and γ-phosphates, which provided excellent Lorentzian fits. The β-phosphate peak fit poorly to a triplet split Lorentzian line shape, and the value of the broadening cannot be ascertained; qualitatively, however, line broadening is definitely observed for the β-phosphate. This inability to quantify line broadening for the β-phosphate is not indicative of any inaccuracy in the resonance frequency: all resonance frequencies were calculated as the center-of-mass of the peak or peaks for a given ^{31}P nucleus, which is entirely independent of the Lorentzian fitting process. The line broadening in the denatured collagen sample is a factor of 1.5−2 smaller than that observed for the samples in which SLS crystallites

were formed and can probably be attributed to the increased solution viscosity and to interaction of some ATP with the collagen random coils, which would retard its motion slightly.

To summarize, the hypothesis that ATP is binding within SLS collagen crystallites is fully upheld by the ^{31}P NMR spectral attributes. Appreciable line broadening is observed within solution state, freely tumbling SLS collagen crystallite samples. Compared to ATP incubated with denatured collagen where the solution viscosity increased in a similar manner and binding between ATP and denatured collagen would occur, the observed line broadening is significantly greater. The line broadening is greatest under the conditions in which the ratio of ATP to collagen is below r^*, when the contribution of free ATP in solution to the ^{31}P NMR signal should be at a minimum. Line broadening in a solution state sample is typically attributed to more efficient transverse relaxation,[53] especially with a non-quadrupolar nucleus such as [31]P. This implies a decrease in mobility of the ATP upon formation of SLS collagen crystallites.

4.2. Bound State of ATP. While a three-dimensional model of the collagen monomer is not yet available, its shape is generally accepted to be rodlike, with a length of ∼280 nm and a diameter of ∼1.5 nm.[41] An analysis of the primary sequence of human type I collagen[42] reveals a number of acidic and basic residues. At the pH of the SLS crystallite assembly, both the acidic and basic residues would be mostly protonated, leading to a large, net positive charge. While a net positive charge toward the N-terminal is predicted even at physiological pH,[55] an examination of the location of the basic residues along the length of the monomer describes a very different picture at pH ∼3.8. Interestingly, the vast majority of the ∼250 basic residues in the triple-helical region are conserved in primary sequence between the α1(I) and α2(I) chains of type I collagen (a tripeptide composed of two α1(I) chains and one α1(II)). This is strictly a one-dimensional analysis of a three-dimensional system; however, it is reasonable to assume that the stringent triple-helical,[43−45] geometry will ensure that each of these conserved sites will lead to a cluster of cationic charge, all of which would be quite accessible to binding. The basic residues appear to be spread quite evenly along the length of the monomer, implying that no particular region of the monomer should be overwhelmingly favored for binding by an anion. For the present, it can be concluded that, while there are definite regions of positive charge in the collagen monomer, these are spread fairly evenly along the surface of the collagen monomer.

An examination of the expected structure of ATP at pH ∼3.8 (Figure 1) shows it to be a zwitterion of net charge ∼−2, with each of the three phosphate groups monovalently anionic, and the adenosine base monovalently cationic.[31−33] Therefore, the anionic phosphate groups will likely bind readily to the cationic basic residues of a collagen monomer. Situating the cationic adenosine base near a cationic region of the collagen monomer would, on the other hand, be unfavorable. At r^*, there are ∼3−4 ATP molecules per positive residue on each collagen monomer, or ∼9−12 anionic ATP groups per cationic collagen group. On the presumption that the binding between ATP and collagen monomer is a charge−charge interaction, this ratio indicates that such binding is readily possible due to the large ratio of highly mobile ATP molecules to cationic binding sites on the less mobile collagen.

Since ^{31}P NMR chemical shifts are dependent upon a multitude of factors, and are not generally predictable,[56,57] a direct analysis of the chemical shifts of each sample is not carried out. This unpredictability was evinced by the experimental variation in the relative location of the spectrum, which

AFM and NMR of Protein−Nucleotide Aggregates

J. Phys. Chem. B, Vol. 106, No. 21, 2002 **5559**

was shifted by ∼20 Hz between the extreme up- and downfield cases. Instead, the following analysis is based upon relative changes in chemical shift. Examining the structure of the triphosphate group of ATP (Figure 1), the following may be inferred. If the γ-phosphate binds to a site upon a collagen monomer, the β-phosphate will be rather restricted in the conformations in which it may favorably bind. However, the same will not be true for the α-phosphate, which will be reasonably free to bind in a variety of conformations. The same will be true if the α-phosphate binds first. However, if the β-phosphate binds first, the α- and γ-phosphates will be restricted in binding conformations. Statistically speaking, more binding events will be likely for the α-/γ-phosphate pair than for the β-phosphate. Furthermore, the γ-phosphate is somewhat freer to bind, due to its relatively unencumbered location furthest from the bulky sugar and base portion of the molecule. A final factor weighing in the favor of the γ-phosphate is that it should have the highest density of negative charge of the three phosphate groups according to its highly acidic nature; the pK_a is not typically reported for this OH group.[31−33]

If a charge−charge interaction is taking place, the O^- of a given phosphate group will be contributing through a decreased electron density around the phosphate, and increased electron density in the cationic group of the collagen monomer. While this likely causes a very small increase to the resonance frequency of the ^{31}P nucleus,[56,57] it should still be discernible. Hydrogen-bonding is also quite likely between the OH or O^- of the phosphate groups and the collagen, but this would likely have a rather minimal effect on the ^{31}P-resonance frequencies compared to a direct anion−cation interaction. Assuming that the β-phosphate is participating less in such electrostatic binding than the α- or the γ-phosphate, the resonance frequency differences for each of the collagen samples, relative to the free ATP sample, should show a downfield shift for the α- and the γ-phosphates in comparison with the β-phosphate. An examination of the data in Table 2 demonstrates exactly this trend.

In all the cases studied, whether SLS crystallite or denatured collagen/ATP solution, an increase in ^{31}P resonance frequency difference between the α- and γ-phosphates and the β-phosphate is seen relative to the average of free ATP samples. Following the presumption of increased binding probability for the α- and γ-phosphates versus the β-phosphate, this implies that an electrostatic interaction is taking place. Due to the nature of the species involved, a direct charge−charge interaction seems most likely. In the case of denatured collagen there should still be many cationic binding sites and the ATP should therefore still have an affinity to form charge−charge interactions. The observation of the same downfield shift pattern of the α- and γ-phosphates vs the β-phosphate in the denatured collagen− ATP sample therefore strengthens the hypothesis of ATP binding to collagen. This observation also strengthens the hypothesis that the greater line broadening shown above for crystallites versus ATP with denatured collagen is primarily due to the restriction in motion by binding within the crystallite structure, as opposed to simply increased viscosity or simple charge−charge binding events with cationic peptide moieties.

4.3. Potential Scaffolding Interactions in the Crystallite. While it is clear from these experiments that ATP is incorporated directly into SLS crystallites, the exact manner by which it serves to stabilize the well-defined SLS crystallite structure is unclear. Following the above analysis, the interaction between collagen and ATP in the SLS collagen crystallite appears to be due to interactions between charged species. Hydrogen-bonding interactions are also likely, but this would be extremely difficult to probe. The electrostatic interaction is amplified for the α- and γ-phosphates over the β-phosphate, as is evident in the observed trend in downfield resonance shifts. This suggests preferential conformations in ATP−collagen binding due to the inherent geometry of the triphosphate moiety. The decrease in mobility of all three phosphate groups, and hence, of the ATP as a whole, demonstrates direct incorporation of the ATP into the SLS collagen crystallite. The location of the cationic base of the nucleotide is another enigma. Whether this is typically bound to a phosphate of another nucleotide, or remains unbound, is entirely unknown. More elaborate experiments upon this system may be envisioned in order to determine the nature of SLS collagen crystallite scaffolding. With the present information, however, the exact nature of the linkages is ambiguous.

5. Conclusions

We have shown that a combination of NMR and AFM has great potential in providing information about mesoscale systems. This parallel use of ^{31}P NMR spectroscopy and AFM demonstrates the first direct proof that ATP is incorporated into the collagen assembly during the formation of SLS collagen crystallites. The incorporation results in a demonstrated restriction of the motion of the triphosphate portion of the ATP. The ATP−collagen interaction in the crystallites is shown herein to likely be occurring, at least in part, through direct charge−charge binding interactions between the anionic phosphate groups and the cationic residues of the collagen. The exact nature of these interactions is still elusive, but should be discernible through continued study.

References and Notes

(1) Evans, J. N. S. *Biomolecular NMR Spectroscopy*; Oxford University Press: Oxford, U.K., 1995.

(2) Wider, G. *Prog. Nucl. Magn. Reson. Spectrosc.* **1998**, *32*, 193−275.

(3) Badia, A.; Lennox, R. B.; Reven, L. *Acc. Chem. Res.* **2000**, *33*, 475−481.

(4) Becker, E. D. *High-resolution NMR: theory and chemical applications*, 3rd ed.; Academic Press: San Diego, 2000.

(5) MacKintosh, F. C.; Schmidt, C. F. *Curr. Opin. Colloid Interface Sci.* **1999**, *4*, 300−307.

(6) Jandt, K. D. *Mater. Sci. Eng., R* **1998**, *21*, 221−295.

(7) Goh, M. C. *Adv. Chem. Phys.* **1995**, *91*, 1−83.

(8) Kiselyova, O. I.; Yaminsky, I. V. *Colloid J.* **1999**, *61*, 1−19.

(9) Bowen, W. R.; Lovitt, R. W.; Wright, C. J. *Biotechnol. Lett.* **2000**, *22*, 893−903.

(10) McLaurin, J.; Yang, D.; Yip, C. M.; Fraser, P. E. *J. Struct. Biol.* **2000**, *130*, 259−70.

(11) Kadler, K. E.; Holmes, D. F.; Trotter, J. A.; Chapman, J. A. *Biochem. J.* **1996**, *316*, 1−11.

(12) Schwarzbauer, J. E.; Sechler, J. L. *Curr. Opin. Cell Biol.* **1999**, *11*, 622−7.

(13) Tzaphlidou, M. *Electron Microsc. Rev.* **1992**, *5*, 25−35.

(14) Barral, J. M.; Epstein, H. F. *Bioessays* **1999**, *21*, 813−23.

(15) Friedhoff, P.; von Bergen, M.; Mandelkow, E. M.; Mandelkow, E. *Biochim. Biophys. Acta* **2000**, *1502*, 122−32.

(16) Hodge, A. J. Structure at the electron microscopic level. *Treatise on collagen*; Academic Press: London, 1967; Vol. 1, pp 185−205.

(17) Fujita, Y.; Kobayashi, K.; Hoshino, T. *J. Electron Microsc.* **1997**, *46*, 321−6.

(18) Paige, M. F.; Rainey, J. K.; Goh, M. C. *Biophys. J.* **1998**, *74*, 3211−6.

(19) Paige, M. F.; Rainey, J. K.; Goh, M. C. *Micron* **2001**, *32*, 341−353.

(20) Paige, M. F.; Goh, M. C. *Micron* **2001**, *32*, 355−361.

(21) Holmes, D. F.; Capaldi, M. J.; Chapman, J. A. *Int. J. Biol. Macromol.* **1986**, *8*, 161−166.

(22) Highberger, J. F.; Gross, J.; Schmitt, F. O. *J. Am. Chem. Soc.* **1950**, *72*, 3321−3322.

(23) Chapman, J. A.; Armitage, P. M. *Conn. Tiss. Res.* **1972**, *1*, 31−37.

(24) Schmitt, F. O.; Gross, J.; Highberger, J. H. *Proc. Natl. Acad. Sci. U.S.A.* **1953**, *39*, 459−470.

(25) Kuhn, K. *Colloid Relat. Res.* **1982**, *2*, 61−80.

(26) Rainey, J. K. Influences of charged and sterically bulky species upon the morphology and structure of preferential aggregates of collagen. M.Sc., University of Toronto, 2000.

(27) Rainey, J. K.; Goh, M. C. Ongoing work.

(28) Kobayashi, K.; Niwa, J.; Hoshino, T.; Nagatani, T. *J. Electron Microsc.* **1992**, *41*, 235−41.

(29) Paige, M. F. Assembly mechanisms of type I collagen aggregates. Ph.D., University of Toronto, 2000.

(30) Rakhit, R.; Lin, A. C.; Paige, M. F.; Goh, M. C. Unpublished results.

(31) Feder, J. *Top. Phosphorus Chem.* **1983**, *11*, 1−18.

(32) Svetlova, I. E.; Smirnova, N. S.; Dobrinina, N. A.; Martinenko, L. I.; Evseev, A. M.; Spitsyn, V. I. *Dokl. Akad. Nauk. S.S.S.R.* **1987**, *294*, 890−893.

(33) Tribolet, R.; Sigel, H. *Eur. J. Biochem.* **1988**, *170*, 617−26.

(34) Goh, M. C.; Paige, M. F. Manuscript in preparation.

(35) Komsa-Penkova, R.; Spirova, R.; Bechev, B. *J. Biochem. Biophys. Methods* **1996**, *32*, 33−43.

(36) Lopez, J. M.; Imperial, S.; Valderrama, R.; Navarro, S. *Clin. Chim. Acta* **1993**, *220*, 91−100.

(37) Na, G. C. *Collagen Relat. Res.* **1988**, *8*, 315−330.

(38) Duhamel, R. C.; Meezan, E.; Brendel, K. *J. Biochem. Biophys. Methods* **1981**, *5*, 67−74.

(39) Galasinski, W.; Gadek, A.; Ratkiewicz, A.; Rzeczycki, W. *Anal. Biochem.* **1978**, *85*, 550−5.

(40) Mayo, K. H. *Biopolymers* **1996**, *40*, 359−70.

(41) Nimni, M. E. *Collagen*; CRC Press: Boca Raton, FL, 1988; Vol. 1.

(42) Using human type I collagen from the Protein Information Resource (Barker, W. C.; et al. *Nucl. Acids Res.* **2001**, 29−32.) α1(I) & α2(I) chains − entry numbers CGHU1S & CGHU2S.

(43) Okuyama, K.; Nagarajan, V.; Kamitori, S. *Proc. Indian Acad. Sci.* **1999**, *111*, 19−34.

(44) Beck, K.; Brodsky, B. *J. Struct. Biol.* **1998**, *122*, 17−29.

(45) Brodsky, B.; Ramshaw, J. A. *Matrix Biol.* **1997**, *15*, 545−54.

(46) Marsolais, F.; Laviolette, M.; Kakuta, Y.; Negishi, M.; Pedersen, L. C.; Auger, M.; Varin, L. *Biochemistry* **1999**, *38*, 4066−71.

(47) Markiewicz, P.; Goh, M. C. *Ultramicroscopy* **1997**, *68*, 215−221.

(48) Ta, T. C.; Sykes, M. T.; McDermott, M. T. *Langmuir* **1998**, *14*, 2435−2443.

(49) Chicon, R.; Ortuno, M.; Abellan, J. *Surf. Sci.* **1987**, *181*, 107−111.

(50) Keller, D. *Surf. Sci.* **1991**, *253*, 353−364.

(51) Mackie, A. R.; Gunning, A. P.; Ridout, M. J.; Morris, V. J. *Biopolymers* **1998**, *46*, 245−252.

(52) Ribeiro, A.; Parello, J.; Jardetzky, O. *Prog. Biophys. Mol. Biol.* **1984**, *43*, 95−160.

(53) Günther, H. *NMR spectroscopy: basic principles, concepts, and applications in chemistry*, 2nd ed.; Wiley: Chichester, New York, 1995; Sections 7.3 and 10.8.

(54) MacDonald, P. M. *Acc. Chem. Res.* **1997**, *30*, 196−203.

(55) Veis, A.; George, A. Fundamentals of interstitial collagen self-assembly. In *Extracellular Matrix Assembly and Structure*; Yurchenco, P. D., Birk, D. E., Mecham, R. P., Eds.; Academic Press: New York, 1994; pp 15−45.

(56) van Wazer, J. R.; Letcher, J. H. *Top. Phosphorus Chem.* **1967**, *5*, 169−226.

(57) Gorenstein, D. G. Phosphorus-31 chemical shifts: Principles and emperical observations. In *Phosphorus-31 NMR − Principles and applications*; Gorenstein, D. G., Ed.; Academic Press: New York, 1984; pp 7−36.